HEFAT2010
7th International Conference on Heat Transfer, Fluid Mechanics and Thermodynamics
19-21 July 2010
Antalya, Turkey

Three-dimensional analysis of mixed convection in a differentially heated lid-driven cubic enclosure

Nasreddine BENKACEM*, Nader BEN CHEIKH
Département de Physique, Faculté des Sciences de Tunis,
Campus Universitaire, 2092 El-Manar II, Tunis, Tunisia
E-mail: ouertatani5000@yahoo.fr

ABSTRACT
To study the intricate three-dimensional flow structures and the companion heat transfer rates in a differentially heated lid-driven cubic cavity, a numerical methodology based on the finite volume method and a full multigrid acceleration is utilized in this note. The four remaining walls forming the cubic cavity are adiabatic. The working fluid is air so the Prandtl number equates to 0.71. Numerical solutions are generated for representative combinations of the controlling Reynolds number inside $100 \leq Re \leq 1000$ and the Richardson number inside $0.001 \leq Ri \leq 10$. Typical sets of streamlines and isotherms are presented to analyze the tortuous circulatory flow patterns set up by the competition between the forced flow created by the moving wall and the buoyancy force of the fluid. Correlations between the average Nusselt number through the cold wall and the Richardson number were established for the mentioned Reynolds numbers.

Keywords: Three-dimensional analysis; lid-driven cubic cavity; mixed convection; numerical simulation; multigrid method.

NOMENCLATURE

H	side of cubic cavity
g	gravitational acceleration
Gr	Grashof number, $g\beta(T_{HOT}-T_{COLD})H^3/\nu^2$
m	iteration level
n	normal direction
Nu	mean Nusselt number
Nu_{loc}	local Nusselt number
p	non-dimensional pressure
p_0	pressure scale, ρu_0^2
Pr	Prandtl number, ν/α
Re	Reynolds number, $u_0 H/\nu$
Ri	Richardson number, Gr/Re^2
t	non-dimensional time
t_0	time scale, H/u_0
T	temperature
T_{COLD}	temperature of cold wall
T_{HOT}	temperature of hot wall
u_0	velocity scale
u, v, w	non-dimensional velocities
x, y, z	non-dimensional cartesian coordinates
α	thermal diffusivity of the fluid
β	coefficient of thermal expansion of the fluid
ν	kinematic viscosity
θ	non-dimensional temperature, $(T-T_C)/(T_H-T_C)$
ρ	density

INTRODUCTION

The problem on laminar mixed convection in cavities has multiple applications in the field of thermal engineering. Such problems are of great interest, for example in electronic device cooling, high-performance building insulation, multi shield structures used for nuclear reactors, food processing, glass production, solar power collector, etc. Numerous studies on lid-driven cavity flow and heat transfer involving different cavity configurations, various fluids and imposed temperature gradients have been continually published in the literature.

The numerical simulations of Moallemi and Jang [1] focused on two-dimensional laminar flow induced by Reynolds number $100 \leq Re \leq 1000$, and small-to-moderate Prandtl number $0.01 \leq Pr \leq 50$ on the flow and heat transfer features in a cavity for different levels of the Richardson numbers. These authors found that the influence of buoyancy on the flow and heat transfer are to be more pronounced for higher values of *Pr,* if *Re* and *Gr* are kept constant.

Sharif [2] performed a numerical investigation with flow visualization of laminar mixed convective heat transfer in two-dimensional shallow rectangular driven cavities of aspect ratio 10. The top moving plate of the cavity is set at a higher temperature than the bottom stationary plate. The fluid Prandtl number is taken as 6, representative of water. The effects of inclination of such a cavity on the flow and thermal fields were also investigated for inclination angles ranging from 0° to 30°. It was concluded that the average or overall Nusselt number increases mildly with cavity inclination for the dominant forced convection case dictated by $Ri = 0.1$. In contrast, it increases much more rapidly with inclination for the other dominant natural convection case dictated by $Ri = 100$.

Prasad et al. [3] numerically studied mixed convection inside a rectangular cavity where the two vertical walls are maintained at cold temperature. In one case, the top-moving wall is maintained at hot temperature and the bottom is at a cold temperature and in the other case, the top is at a cold temperature and the bottom is at a hot temperature. They concluded that when the negative *Gr* is increased, a strong convection is manifested for aspect ratios equal to 0.5 and 1.0. Even more, a Hopf bifurcation occurs at $Gr = -10^5$ for the aspect ratio 2.

Mohammad and Viskanta [4] numerically examined two and three-dimensional laminar flow and heat transfer in a Rayleigh-Bénard container. They established that the lid motion annihilates all forms of convective cells due to heating from below for finite size cavities. Aydin et al. [5] conducted a numerical investigation to analyze the transport mechanism of mixed convection in a shear and buoyancy-driven cavity having a locally heated lower wall and moving cooled sidewalls. In addition, other numerical studies such as Han and Kuehn [6] and Oztop and Dagtekin [7] were carried out on this topic.

Iwatsu et al. [8] performed a numerical investigation on the effect of external excitation on the flow structure in a square cavity. The results have shown similar flow structure to steady driven-cavity flows when utilizing small frequency values. Such a similarity, however, vanished when large frequency values were implemented. A subsequent work by Iwatsu et al. [9] carried out a numerical study of the viscous flow in a heated driven-cavity under thermal stratification, where the oscillating lid was maintained at a temperature higher than the lower wall. Their collection of results had revealed significant augmentation in heat transfer rate at particular lid frequency values, which convincingly indicates the existence of the resonance phenomena.

A detailed literature survey reveals that the majority of existing numerical investigations are restricted to two dimensional configurations. In this vein, 2D models are deficient because they do not always realistically capture the intricacies inherent to the flow behaviour. Because of these shortcomings, 3D models have to be undertaken to guarantee accuracy. A limited number of articles falls into this general category and has been reported in the literature. Among others, Iwatsu [10] numerically studied three dimensional mixed convective flows in a cubical container with a steady vertical temperature stratification. He observed that the three dimensional effects are intensified as *Re* increases. Mohammad and Viskanta [11] conducted three- dimensional numerical simulation of mixed convection in a shallow driven cavity heated from the top moving wall and cooled from below. The cavity was filled with a stably stratified fluid encompassing a relative large range of Rayleigh and Richardson numbers. In a consecutive number of papers, Freitas et al. [12] and Freitas and Street [13] carried out a numerical study of the viscous flow in a rectangular cavity of depth- to- spanwise aspect ratio 3 at $\mathrm{Re}=3200$. They discovered the existence of meridional vortices and considerable flow unsteadiness.

In view of the foregoing statements, it seems that the problem of three dimensional laminar mixed convection heat transfers in a differentially heated lid-driven cubic cavity has not been addressed yet. In this paper, we undertake this task varying the Reynolds number in the *Re*-interval $(100 \le \mathrm{Re} \le 1000)$ and the Richardson number in the *Ri*- interval $(0.001 \le Ri \le 10)$ for air (*Pr* = 0.71) as the working fluid. The transport processes will be investigated with the finite volume method and the discussion will revolve around the precise determination of steady velocity and temperature fields. In addition, the average Nusselt number will be documented for all cases studied.

The paper is organized as follows: in the second section the physical system is formulated; the numerical methodology is briefly described in the third section and subsequently validated. The computed results are presented and discussed in the fourth section. In the final section, the most important findings of this study are summarized.

2. Physical system

The physical system under study is sketched in Fig. 1. It basically consists of a cubic cavity with side H filled with air $(\mathrm{Pr}=0.71)$. The applicable flow and temperature boundary conditions are described next. The top lid imparts a steady sliding motion with a uniform velocity u_0, while the other walls are stationary. The cavity is differentially heated over the vertical sides. The left hot wall has a temperature T_{HOT} and the right cold wall has a temperature T_{COLD} wherein $T_{HOT} > T_{COLD}$. In addition, the remaining walls are considered adiabatic.

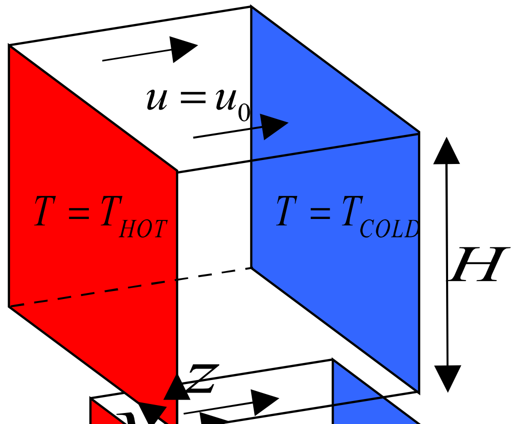

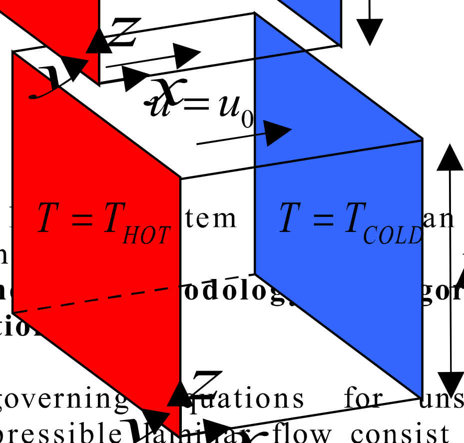

Fig. 1. ... tem ... an ... coordin...

3. Num... odolog... gorithm validatio...

The governing ...uations for unsteady, incompressible ... flow consist of the continuity equation, the Navier–Stokes equations accounting for the Boussinesq approximation and the energy equation.

The non-dimensional equations are collectively written in tensor notation as follows:

Continuity equation:

$$\frac{\partial u_i}{\partial x_i} = 0,$$
(1)

Three Momentum equations:

$$\frac{\partial u_i}{\partial t} + \frac{\partial (u_i u_j)}{\partial x_j} = -\frac{\partial p}{\partial x_i} + \frac{1}{\mathrm{Re}}\left(\frac{\partial^2 u_i}{\partial x_i \partial x_i}\right) + Ri\theta\ \delta_{i3},$$
(2)

Energy equation:

$$\frac{\partial \theta}{\partial t} + \frac{\partial (u_i \theta)}{\partial x_i} = \frac{1}{Ra\mathrm{Pr}}\left(\frac{\partial^2 \theta}{\partial x_i \partial x_i}\right)$$
(3)

where $u_i = (u; v; w)$ are the velocity components, p is the kinematic pressure, and θ is the temperature, ρ is the mass density, and g is the gravitational acceleration. In Eq. (2), the symbol δ_{ij} stands for the Krönecker delta. The chosen scales in Eqs. (1)-(3) are the side H, the velocity $u_0 = \sqrt{g\beta H \Delta T}$, the time $t_0 = H/u_0$ and the pressure $p_0 = \rho u_0^2$. Further, the non-dimensional temperature is defined by $\theta = \frac{T - T_R}{T_{HOT} - T_{COLD}}$, where the reference temperature $T_R = \frac{T_{HOT} + T_{COLD}}{2}$ and the temperature scale is the lid-to-lid temperature difference $T_{HOT} - T_{COLD}$.

As presented above, the forced-natural convection problem is characterized by three non-dimensional parameters: 1) the Reynolds number $\mathrm{Re} = \frac{u_0 H}{\nu}$ where u_o is the impressed lid velocity; 2) the Prandtl number $\mathrm{Pr} = \frac{\nu}{\alpha}$, where ν is the kinematic viscosity, α the thermal diffusivity of the fluid; 3) the Grashof number $Gr = \frac{\beta g \Delta T H^3}{\nu^2}$ in which β is the coefficient of thermal expansion of the fluid, g the gravity and $\Delta T = T_{HOT} - T_{COLD}$ the temperature difference between the hot and cold horizontal walls. Alternatively, Gr and Re are adequately blended in the mixed-convection parameter called the Richardson number $Ri = \frac{Gr}{\mathrm{Re}^2}$.

The unsteady Navier–Stokes and energy equations are discretized by a second-order time stepping finite difference procedure. The procedure adopted here deserves a detailed explanation. First, the non-linear terms in Eqs. (2) are treated explicitly with a second-order Adams–Bashforth scheme. Second, the convective terms in Eq. (3) are treated semi-implicitly. Third, the diffusion terms in Eqs. (2) and (3) are treated implicitly. In order to avoid the difficulty that the strong velocity-pressure coupling brings forward, we selected a projection method described in Peyret and Taylor [14] and Achdou and Guermond [15].

A finite-volume method is implemented to discretize the Navier–Stokes and energy equations (Patankar [16], F. Moukhalled and M. Darwish [17], Kobayachi and Pereira and Pereira [18]). The advective terms in Eqs. (2) are discretized using a QUICK third-order scheme whereas a second-order central differencing (Hayase, Humphrey and Greif [19]) is applied in Eq. (3). The discretized momentum and energy equations are solved employing the red and black successive over relaxation method (RBSOR) in Press et al. [20], while the Poisson pressure correction equation is solved utilizing a full multi-grid method (Hortmann, Peric and Scheuerer [21], M.S. Mesquita and M. J. S. de Lemos [22], E. Nobile [23]). If specific details about the computational methodology are needed, the reader is directed to Ben Cheikh et al. [24]. Finally, the convergence of the numerical 3D velocity field and the 3D temperature field is established at each time step when all residuals are forced to stay below 10^{-6}. To secure steady state conditions the following criterion has to be satisfied:

$$\sum_{i,j,k}\left|\Phi_{i,j,k}^{m+1}-\Phi_{i,j,k}^{m}\right|\leq 10^{-5} \quad (4)$$

where the generic variable Φ represents the set of four variables u,v,w or θ. In the above inequality, the superscript m indicates the iteration number and the subscript sequence (i,j,k) represents the space coordinates x, y, z.

For enhanced accuracy, the present numerical model was checked against the published numerical solution of E. Tric [25]. The outcomes of the one-to-one comparisons are documented in Table 1 for the average Nusselt number predictions and maximum velocities. It is observed here that the present numerical computations match very closely those of [25].

A second comparison to those of Iwatsu [10] relatively to a 3D mixed convection was undertaken. As shown in Table 2, good agreements are evident with respect to the result reported by [10].

Table 1
Comparison of the computed average Nusselt number predictions and maximum velocities

	$Ra = 10^4$			$Ra = 10^5$		
	Tric [25]	Pres. Work	Err %	Tric [25]	Pres. Work	Err %
Grille	81^3	48^3		81^3	48^3	
u_{max}	16.719	16.634	-0.51	43.90	44.06	0.36
v_{max}	2.156	2.136	-0.93	9.69	9.55	-0.15
w_{max}	18.983	18.942	-0.22	71.06	70.85	-0.30
Nu_{mp}	2.250	2.247	-0.13	4.612	4.605	-0.15
Nu_{3D}	2.054	2.054	0	4.337	4.332	-0.

Table 2
Comparison of our results with [10]

Re	*Ri* =0.001		*Ri* =1.0		
	Ref [10]	Pres. Work	Ref [10]	Pres. Work	Ref [1
100	1.82	1.836	1.33	1.348	1.08
400	3.99	3.964	1.50	1.528	1.17
1000	7.03	7.284	1.80	1.856	1.37

4. Results and discussion

The computed mixed convection flow and temperature fields in the lid-driven cubic cavity are examined in this section. The numerical results are presented in terms of streamlines and isotherms. The Reynolds number *Re* is varied two orders of magnitude between 100 and 1000. In addition, the Richardson number *Ri* is varied four orders of magnitude between 0.001 and 10. The Prandtl number is set at *Pr* = 0.71. We ran computations for nine different pairs of *Ri* and *Re*; that is: (*Ri*, *Re*) = (10, 100), (10, 400), (10, 1000), (1, 100), (1, 400), (1, 1000), (0.001, 100), (0.001, 400) and (0.001, 1000). In harmony with this, the implications of varying *Ri* and *Re* will be adequately highlighted.

A series of trial calculation were conducted with two different variable grid distributions, i.e., 48×48×48 and 64×64×64. For the moderate case dealing with *Re* = 400 and *Ri* = 1.0, minor differences of less than 0.25% were detected between the flow and temperature results produced by the grid 48×48×48 and those by the grid 64×64×64. Consequently, to optimize the grid distribution appropriately, the grid 48×48×48 was deemed adequate to perform all numerical computations. For completeness, the two grids were built using a tangent hyperbolic formulation. The smallest space intervals chosen in the three coordinate directions are $\Delta x_{min} = \Delta y_{min} = \Delta z_{min} = 2.25\times10^{-3}$, and are localised near the moving and stationary walls to capture the growth of the flow and thermal boundary layers adjacent to them. The time step was set to $\Delta t = 0.01$ for all computations.

The mid-plane streamlines distributions for designated values of *Re* and *R*i are displayed in Fig. 2. We note that for the lowest Richardson number employed (*R*i =0.001), the trajectory of fluid particles is very similar to that corresponding to the classical lid-driven cavity [26] (see Fig. 2a-2d-2g). Indeed, Fig. 2a shows the flow structure in the cavity at *Re*=100 with a primary vortex occupying the main part of the cavity. Two small recirculation cells are also emerging at the bottom corners as the Reynolds number goes through Re=400 to Re=1000.

When *Ri* is large (*Ri*=10), it is noticeable in Fig. 2c (*Re*=100) the presence of two eddies localised in the proximity of the core region. With increments in *Re*, the right cell becomes feeble and amalgamates with the left one to provide only one stretched vortex. Interestingly, it is also noticed when *Re*=1000, that the direction of the lid velocity causes the centre of the vortex to move from the left side to the right side as confirmed by figure 2i.

The case (*Ri*=1; *Re*=100) is very similar to (*Ri*=0.001; *Re*=100). In fact a primary cell is observed in the cavity with a little difference that its center is slightly moved downward. It is conspicuous in Fig.2e the effect of increasing the Reynolds number (*Re*=400) on the flow structure. The main vortex moves down and is somewhat dragged to the right side of the cold wall. For *Re*=1000, the high lid velocity causes the division of the main vortex in two cells (see Fig.2h).

The qualitative features of the temperature field are demonstrated by plotting the perspective views of isotherms, as reflected in Fig. 3. In fact, it is clearly discernible from the patterns of isotherms that, for the feeble value of Richardson number (*Ri*=0.001), the mechanically driven forced convection dominates the buoyancy-driven convection (Fig. 3a,3d and 3g), implying that the forced convection is essentially due to the lid-movement. In contrast, as *Ri* increases to *Ri*=10 the buoyant convection distorts the isotherm fields and three-dimensional patterns become more pronounced when *Re* increases (Fig.3c, 3f and 3i). The distortion of the isotherm field increases with Richardson number. In other words, the flow is principally dominated by buoyancy and the heat transfer is controlled mainly by natural convection, signifying that the forced convection due to the lid-movement is almost absent.

For *Ri*=1, a compromise between the two phenomena, evoked previously, is clearly seen in figures 2b, 2e, 2h, 3b, 3e and 3h.

In order to assess the average heat transfer distribution along the vertical walls, the Nusselt number is introduced and is defined by: $Nu = \int_0^1 \int_0^1 -\frac{\partial\theta}{\partial x}\Big|_{x=0\ or\ x=1} dydz$.

Table 3 lists the average Nusselt number *Nu* at the cold and hot walls for the computations obtained for the nine combinations (Re, Ri) studied.

The results convincingly indicate that when *R*e is small (*Re*=100), the heat transfer through the cold and the hot walls exhibit similar trends for each value of *Ri*. For this same Reynolds number, the average Nusselt number increases with the Richardson number. By increasing the Reynolds number, values of Nusselt number increase and small differences between Nu_{hot} and Nu_{cold} are observed. When *Ri* is small at high values of *Re*, the difference between Nu_{hot} and Nu_{cold} augment.

Relatively to the heat transfer through the cold wall, a correlation between *Nu* and *Ri* was established. In fact, several computations (for each Reynolds number) demonstrate clearly the existence of a relation expressed as: $Nu = a \times Ri^{\alpha} + b$. Table 4 lists the values of coefficients a , b and α.

Re	Ri=0.001 (Nu_{hot};Nu_{cold})	Ri=1.0 (Nu_{hot};Nu_{cold})	Ri=10.0 (Nu_{hot};Nu_{cold})
100	(2.1714 ; 2.1714)	(2.6876 ; 2.6876)	(4.3186; 4.3187)
400	(4.3276; 4.3285)	(5.7232 ; 5.7241)	(9.6408 ; 9.6420)
1000	(6.6252 ; 6.6294)	(9.3182 ; 9.3236)	(15.8457 ; 15.8520)

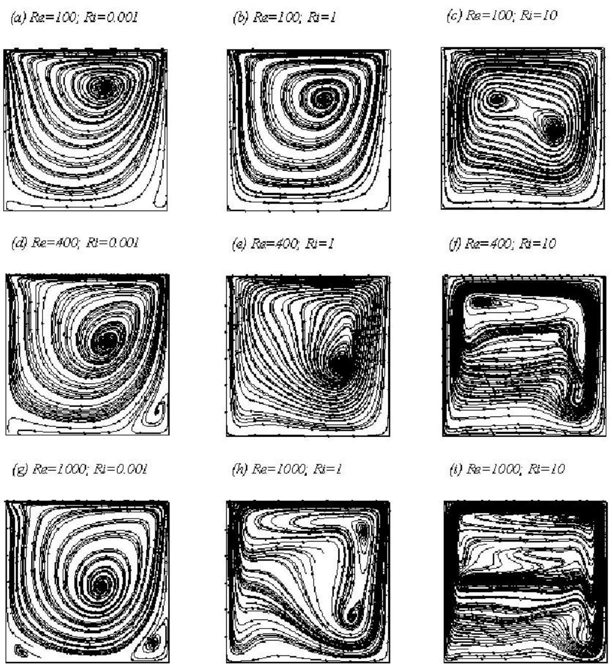

Fig. 2. Trajectory particles at the *x*-*z* mid-plane for different combinations of *Re* and *Ri*.

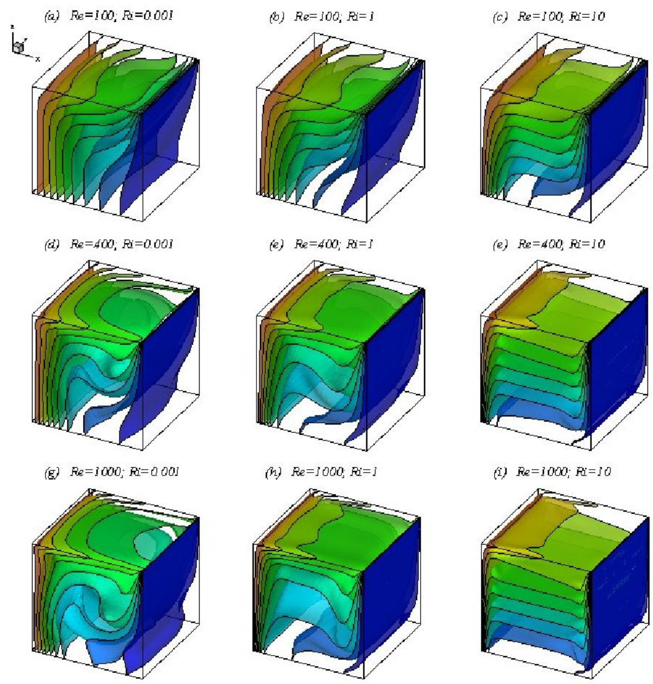

Fig. 3. Isotherm plots for different combinations of *Re* and *Ri*.

Table 3
The average Nusselt number Nu at the cold and hot walls

5. Conclusions

The current investigation addressed three-dimensional laminar mixed convection in a lid-driven cubic cavity filled with air (Pr = 0.71) for suitable combinations of three different Reynolds numbers and three different Richardson numbers. The effects of varying both Reynolds and Richardson numbers on the resulting convection are investigated. Interesting behaviours of the flow and thermal fields with varying Reynolds and Richardson numbers are observed.

When small *R*i is united with low *R*e, a primary vortex is observed occupying the main part of the cavity and its intensity is slightly modified when *R*e increased. In addition, two minor secondary recirculating vortices are observed at the bottom corners as the Reynolds number goes through *Re*=400 to *Re*=1000. Furthermore, three dimensionalities of the isotherm patterns are manifested. In this case, the mechanically driven forced convection dominates the buoyancy- driven, implying that forced convection is essential due to the lid- movement

When large *R*i is paired with low *R*e, two primary vortex are observed in the proximity of the core region and their intensity is considerably modified to provide only one stretched vortex when *R*e increase. It is also seen that the buoyancy-driven dominates the mechanically driven forced convection.

The heat transfer characteristics inside the cubic cavity are improved significantly for low values of *R*i due to the dominant effect of the mechanical effect provoked by the moving lid. The effects of both *Re* and *R*i are also apparent in the values of the average Nusselt number. For high *R*i united with large *Re*, the overall heat transfer and the convection mode dominates the picture. Finally for Reynolds number ranging from 100 to 1000, a correlation between the averaged heat transfer (*Nu*) and *Ri* has been reported.

REFERENCES

[1] M. K. Moallemi, K. S. Jang, Prandtl number effects on laminar mixed convection heat transfer in a lid-driven cavity, Int. J. Heat Mass Transfer 35 (1992) 1881- 1892.

[2] M. A .R. Sharif, Laminar mixed convection in shallow inclined driven cavities with hot moving lid on top and cooled from bottom, Applied Thermal Engineering 27 (2007) 1036- 1042.

[3] Y. S. Prasad, M. K. Das, Hopf bifurcation in mixed flow inside a rectangular cavity, Int. J. Heat Mass Transfer 50 (2007) 3583- 3598.

[4] A.A. Mohammad, R.Viskanta, Laminar flow and heat transfer in Rayleigh- Benard convection with shear, Phys. Fluids A 4 (1992) 2131- 2140.

[5] O. Aydin, W.-J. Yang, Mixed convection in cavities with a locally heated lower wall and moving sidewalls, Numer. Heat Transfer, Part A: Applications 37 (2000) 695- 710.

[6] H. Han, T. H. Kuehn, A numerical simulation of double diffusive convection in a vertical rectangular enclosure, ASME HTD 107 (1989) 149- 154.

[7] H. F. Oztop, I. Dagtekin, Mixed convection in two sided lid driven differentially heated square cavity, Int. J. Heat Mass Transfer 47 (2004) 1761- 11769.
[8] R. Iwatsu, J.M. Hyun, K. Kuwahara, Numerical simulation of flows driven by a torsionally oscillating lid in a square cavity, J. Fluids Engineering. 114 (1992) 143–151.
[9] R. Iwatsu, J.M. Hyun, K. Kuwahara, Convection in a differentially- heated square cavity with a torsionally- oscillating lid, Int. J. Heat Mass Transfer 35 (1992) 1069–1076.
[10] R. Iwatsu, Three- dimensional driven- cavity flows with a vertical temperature gradient, Int. J. Heat Mass Transfer 38, (1995) 3319- 3328.
[11] A.A. Mohammad, R. Viskanta, Flow and heat transfer in a lid- driven cavity filled with a stably stratified fluid, Appl. Math. Modelling 19 (1995) 465–472.
[12] C. J. Freitas, R. L. Street, A. N. Findikakis and J. R. Koseff, Numerical simulation of three-dimensional flow in a cavity, Int. J. Numer. Meth. Fluids 5, (1985) 561- 575.
[13] C. J. Freitas and R. L. Street, Non- linear transport phenomena in a complex recirculating flow: a numerical investigation, Int. J. Numer. Meth. Fluids 8, (1988) 769- 802.
[14] R. Peyret, T. D. Taylor, Methods for Fluid Flow, Springer- Verlag, Berlin, Germany, 1983.
[15] Y. Achdou, J. L. Guermond, Convergence analysis of a finite element projection/ Lagrange–Galerkin method for the incompressible Navier–Stokes equations, SIAM J. Numer. Anal. 37 (2000) 799–826.
[16] S. V. Patankar, A calculation procedure for two-dimensional elliptic situations, Numer. Heat Transfer 34 (1981) 409–425.
[17] F. Moukhalled, M. Darwish, A unified formulation of the segregated class of algorithm for fluid flow at all speeds, Numer. Heat Transfer, Part B: Fundamentals 37 (2000) 103–139.
[18] M. H. Kobayachi, J. M. C. Pereira, J. C. F. Pereira, A conservative finite- volume second- order-accurate projection method on hybrid unstructured grids, J. Comput. Phys. 150 (1999) 40–75.
[19] T. Hayase, J.A.C. Humphrey, R. Greif, A consistently formulated QUICK scheme for fast and stable convergence using finite- volume iterative calculation procedures, J. Comput. Phys. 98 (1992) 108–118.
[20] W. H. Press et al., Numerical Recipes in Fortran 77: The Art of Scientific Computing, vol. 1, second edition, Cambridge Press, London, UK, 1997.
[21] M. Hortmann, M. Peric, G. Scheuerer, Finite volume multigrid prediction of laminar natural convection: benchmark solutions, Int. J. Numer. Meth. Fluids 11 (1990) 189–207.
[22] M.S. Mesquita, M. J. S. de Lemos, Optimal multigrid solutions of dimensional convection-conduction problems, Appl. Math. Comput. 152 (2004) 725–742.
[23] E. Nobile, Simulation of time- dependent flow in cavities with the correction multigrid method, Part I: mathematical formulation, Numer. Heat Transf., Part B: Fundamentals 30 (1996) 341–350.
[24] N. Ben Cheikh, B. Ben Beya, T. Lili, Benchmark solution for time- dependent natural convection flows with an accelerated full- multigrid method, Numerical Heat Transfer, Part B: Fundamentals, 52, (2007) 131–151.
[25] E. Tric, G. Labrosse, M. Betrouni, A first incursion into the 3D structure of natural convection of air in a differentially heated cubic cavity, from accurate numerical solutions, Int. J. of Heat and Mass Transfer, 43, (2000), 4043 –4056
[26] K. L. Wong1; and A. J. Baker2, A 3D incompressible Navier–Stokes velocity–vorticity weak form 2nite element algorithm, Int. J. Numer. Meth. Fluids, 38, (2002) 99–123